A Novel U-Shaped Parasitic Asymmetric Microstrip Cap Loaded Compact Patch Antenna

M. R. Zaman [1], M. T. Islam [2], and Salehin Kibria [1]

[1] Centre for Space Science (ANGKASA)
[2] Dept. of Electrical, Electronic and Systems Engineering, Faculty of Engineering and Built Environment
Universiti Kebangsaan Malaysia, UKM Bangi, 43600, Malaysia
robelhk@yahoo.com, titareq@yahoo.com, sakib2005@yahoo.com

Abstract ─ A novel electromagnetically short antenna with parasitic microstrip cap shape is shown in this paper. The antenna is composed of a U-shaped parasitic microstrip line (cap) excited by coupling with the feed line at patch. The antenna is fabricated in FR4 substrate with dielectric constant, Ɛr=4.55 and thickness of 1.6 mm. Optimization of the proposed antenna is done using modified Particle Swarm Optimization (PSO) algorithm in ZELAND IE3D software environment. That gives resonance at selected frequencies and increased gain than the initial design. By using circular slot at the ground plane with miniaturized structure, dual-band covering 5.29 GHz to 5.89 GHz (C-band) and 7.93 GHz to 8.86 GHz (X-band) is achieved. A fractional bandwidth of 10.74% at C-band and 11.08% at X-band is achieved. A measured gain of 5.65 dBi and 6.61 dBi is achieved at C-band and X-band respectively, with a circular polarization. Gain improvement is achieved compared to the initial design by more than 2 dBi (average) in the selected frequency for the given resonance using modified PSO optimization.

Index Terms ─ C-band, coupled line, optimization, PSO, U-shape, X-band.

I. INTRODUCTION

Modern multiband antenna designs are getting more into different microstrip structures [1-10] due to multiple applications using different frequencies are put together in one system nowadays. To improve the size compatibility with the mobile device, antenna structures are miniaturizing gradually with extensive research. Different types of antennae such as helical, monopole, loop antennae are designed to achieve multiband response in miniaturized volume [1-4]. Due to the size limitation inside the body of mobile devices, the antenna structure becomes more complex. Moreover, the antenna structure tends to be more close to the other parts of the mobile which leads to low resistance and high reactance at the input impedance behaving like an ILA (Inverted L shaped antenna) [5].

In [6], a printed planar antenna for wideband application is shown the antenna is composed of a square patch. However, there is a notch from 4.7 GHz to 5.8 GHz where the antenna is not applicable. In [7], a multiband fractal Sierpinski Gasket antennas' behavior is explained using iterative method. In that research, a basic structure, equilateral triangle is used as sample model. A multiband antenna with resonance response for different application is shown in [8]. The antenna maintains Chebyshev distribution method for slot arrays combined with a triangle shaped patch. The antenna has a relatively large size. To use the same antenna in different applications, switches are installed in a pentagon shaped patch antenna in [9]. In the design, while all the switches are turned on, the resonance shifts a little. A patch antenna with a shape of triangle is explained in [10]. A slot of rectangular shape is cut in the ground plane which can be changed to have different gap size between the two resonant frequencies of the dual-band antenna. To design this triangle shaped patch antenna, a substrate is used with dielectric constant of 1.38 which is not available and not chip compared to FR4 (Fibre-Reinforced plastic) substrates. Planar UWB antenna with Multi-Slotted ground plane is shown in [11]. With a size of 30*22

Submitted On: June 21, 2013
Accepted On: September 26, 2014

mm^2, the antenna bandwidth ranges from 2.57 GHz till 16.72 GHz. However, the gain is very limited within the operating frequency. A metallized dielectric loading technique is shown to achieve multiband behavior in [12]. In this antenna design while the dielectric material is used at the top, the peak gain intends to decrease more than 1.2 dB at the achieved resonance frequencies. Another antenna for L-band application is designed and fabricated using high dielectric constant substrate (ε_r=10.02) to have reasonable axial ratio bandwidth at 1.575 GHz [13]. The simulation results of the antenna indicated that, with the change of the size of the ground plane, the impedance bandwidth of the antenna will significantly change. A triangular patch Yagi antenna is shown in [25] to have reconfigurable characteristics. Two parasitic patches are used to direct the beam of the antenna by using switches on top of them. Another multiband/UWB antenna is shown in [26]. The antenna is composed of two radiating patch along with a 'T' and butterfly shaped stub in the middle of the ground plane. The stub is introduced to have notch in the UWB characteristics. Inductive loading technique is shown in [27] to convert a dual-band antenna into wideband antenna. The bandwidth is enhanced by loading inductive stub component at the ring of the proposed antenna. The measurement result of the antenna shows wider performance than the simulation result. Two L-shaped ground planes are introduced in [28] to have triple band operation in a coplanar waveguide feed antenna. They have also introduced L-shaped and I-shaped slots at the ground plane and radiating patch respectively. However, the peak gain of the antenna is below 2 dBi at most of the operating bands. A circular ring antenna for UWB application is shown in [30] with a compact size of 26*28 mm^2. The antenna has a bandwidth of 14 GHz. However, the antenna gain is minimal at the operating frequency. A coplanar antenna working at 3.53 GHz to 9.5 GHz is shown in [31]. The maximum gain of the antenna is 3.5 dBi with a stable radiation pattern. For antenna performance enhancement, a split ring slotted EBG structure is shown in [32]. By using such design structure as another version of modified ground plane, antenna performance can be enhanced.

Particle Swarm Optimization (PSO) technique is being used widely day by day in designing Electromagnetic structures [14]. PSO is a strong and evolutionary computation technique based on the intelligent swarms' movement. Dual-band/multiband patch antennae, periodic structures, correlator antenna arrays, aperiodic antenna arrays are designed in [15] using PSO. The designs achieved using PSO are fabricated and the measured results tend to agree with the simulated result using the software UCLA antenna lab. A Yagi-Uda antenna design is optimized using BBO and PSO algorithm combined [16]. The paper is more devoted into comparison between two optimization process rather than discussing about the antenna characteristics. A combination of Genetic Algorithm (GA) and PSO is shown in [17]. It shows the optimization of feed-point of microstrip antenna.

In this paper, a dual-band antenna is designed and fabricated with resonance response at the frequencies 6.18 GHz and 8.52 GHz in FR4 substrate. Coupled line cap (CLC) is used to surround the active rectangular patch. By changing the dimension of the cap, the impedance is matched for higher bandwidth. The antenna ground plane is modified using a circular slot centered at the middle with a rectangle shape microstrip line at the center of the slot. The lower resonance frequency shown in the current distribution graph is found by the separated rectangle in the ground plane [18]. Another antenna is designed and fabricated using modified Particle Swarm Optimization (PSO) algorithm which gives the antenna a changed shape with long hands at one side of the CLC and another side is minimized. The PSO algorithm shows similarity with the existing design. By using PSO, increased bandwidth is achieved with almost the same structure at the patch of the antenna without changing the outer dimension (20 mm×20 mm) of the antenna using FR4 substrate with a thickness of 1.6 mm. The proposed patch antenna is designed in FR4 substrate with a compact size lengthening 0.41λ and a width of 0.41λ.

II. ANTENNA DESIGN

Figure 1 shows the structure of the antenna with the parameters tabulated in Table 1.

The boundary conditions for the fields of the dielectric-conductor and conductor-air can be found using Maxwell's equations [19]:

$$\oint_s D.dS = Q_{fce}\,, \tag{1}$$

$$\oint_s E.dl = 0\,, \tag{2}$$

where, Q_{fce} is the free surface charge. The conductor used in the antenna is copper "Cu" which is high in terms of electrical and thermal conductivity, resulting to have $\rho_c \rightarrow 0$ and $\sigma \rightarrow \infty$ which tends to a perfect conductor. The conductor and dielectric substrates interface of the antenna is shown in Fig. 1. The electric field, E=0 at the inside of the conductor. There is an electric field, normal to the conductor throughout the interface of the conductor-dielectric and conductor-air (in the case of air the dielectric constant is '1', so the calculation for electric field is the same as for other dielectric substrates with different dielectric constants) and is external to the conductor.

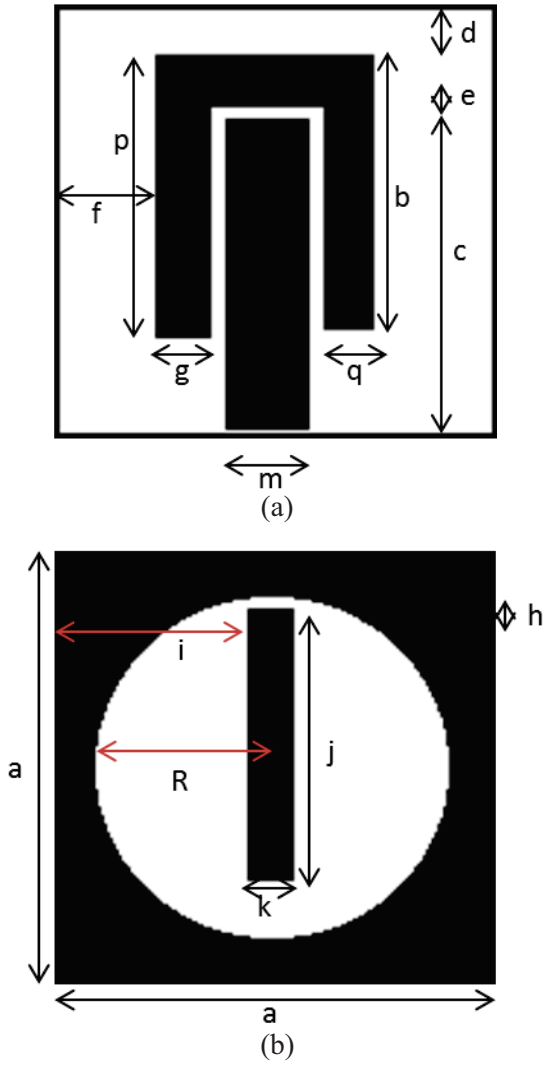

Fig. 1. (a) Patch of the proposed antenna, and (b) ground plane of the proposed antenna.

In Fig. 2, the coupling element that is not connected with the primary patch, electrically partially screens the primary patch. A slit is cut between one microstrip tree and leaf. The characteristics of coupled lines can be applied for the coupling element surrounding the primary patch. From the current distribution of the patch at the later part of this paper, the occurrence of coupling of the primary and coupling element can be observed.

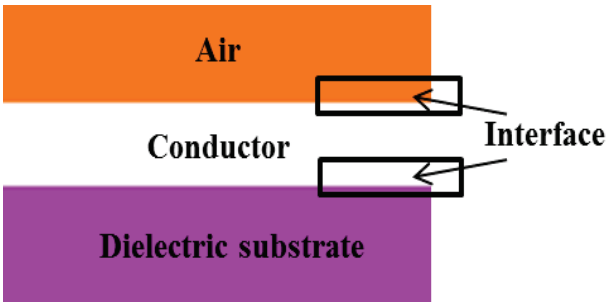

Fig. 2. Antenna material lairs distribution.

The coupling depends on the even and odd mode characteristic impedances of the coupled microstrip lines and vice versa. There are no precise analytic formula which can be applied to the structure shown, whereas approximated formulas can be used to characterize using characteristic impedance (Z_0), even mode impedance (Z_{0e}) and odd mode impedance (Z_{0o}). For the coupled lines with two modes of current flow (electromagnetic consideration), which are due to the ground plane conductor and the displacement of the current coupling between two conductors are specified as differential mode current which is related to Z_{0o}. The energy between the coupled lines flows from the source structure (primary patch) to the matched load structure (coupling element). Due to the thickness of the coupling conductors (minor capacitance), mutual capacitance and ground plane to coupling lines capacitance and distortion due to coupling of each other, the 4 capacitance values for the odd mode is resulting. By considering the magnetic fields, the inductance values can be said to follow the argument. For a non-dissipative system the following equation can be applied:

$$Z_0 = \sqrt{\frac{L(\text{inductance per meter})}{C(\text{capacitance per meter})}}. \qquad (3)$$

For the quarter wavelength matched line, the even and odd mode impedances can be formulated as:

$$Z_{0e} = Z_0\sqrt{\frac{1+k}{1-k}}, \tag{4}$$

$$Z_{0o} = Z_0\sqrt{\frac{1-k}{1+k}}, \tag{5}$$

where, k=10-0.05C, C=coupling between two microstrip lines in dB. From (4) and (5),

$$Z_0 = \sqrt{\frac{Z_{0o}}{Z_{0e}}}. \tag{6}$$

Tracking back, the values of 'L' and 'C' can be found. The coupled structures even (Z_{oe}) and odd (Z_{oo}) mode impedance can be evaluated by using coupled line microstrip structure impedance formulation technique described in [24]:

$$(Z_{0e})_{n-1,n} = \frac{1}{y_0}\left[1+\frac{J_{n-1,n}}{Y_0}+\left(\frac{J_{n-1,n}}{Y_0}\right)^2\right], \tag{7}$$

$$(Z_{0o})_{n-1,n} = \frac{1}{y_0}\left[1-\frac{J_{n-1,n}}{Y_0}+\left(\frac{J_{n-1,n}}{Y_0}\right)^2\right]. \tag{8}$$

With the gap becoming narrower (as small as 0.5 mm for this design), it is more likely for the Z0e to increase due to increment in inductance and decrement in capacitance. As the gap between coupled lines becomes smaller, the field between the common ground of the coupled lines becomes narrower which can be seen in Fig. 3. The eddy current effect can be seen for the electric currents induced within the coupling conductors creating the magnetic field in the middle. The equivalent circuit of a microstrip coupled line gap discontinuity is shown in Fig. 4 [20]. The values for the circuit elements can be calculated using the equations stated below:

$$C_{11} * \frac{25Z_0}{h} = \left[1.125\tanh\left(1.358\frac{W}{h}\right)-0.315\right] \tanh\left[\begin{array}{l}\left(0.0262+0.184\frac{h}{W}\right)+\\ \left(0.217+0.0619\ln\frac{W}{h}\right)\frac{S}{h}\end{array}\right], \tag{9}$$

$$C_{12} * \frac{25Z_0}{h} = \left[6.832\tanh\left(0.0109\frac{W}{h}\right)+0.910\right] \tanh\left[\begin{array}{l}\left(1.411+0.314\frac{h}{W}\right)+\\ \left(\frac{S}{h}\right)^{1.248+0.360\tan^{-1}\frac{W}{h}}\end{array}\right], \tag{10}$$

$$L_{11} * \frac{25}{hZ_0} = \left[0.134+0.0436\ln\frac{h}{W}\right] \exp\left[\begin{array}{l}-1\left(3.656+0.246\frac{h}{W}\right)\\ \left(\frac{S}{h}\right)^{1.739+0.39\ln\frac{W}{h}}\end{array}\right], \tag{11}$$

$$L_{12} * \frac{25}{hZ_0} = \left[0.008285\tanh\left(0.5665\frac{W}{h}\right)+0.0103\right] + \left[0.1827+0.00715\ln\frac{W}{h}\right] \exp\left[\begin{array}{l}-1\left(5.207+1.283\tanh\left(1.656\frac{h}{W}\right)\right)\\ \left(\frac{S}{h}\right)^{0.542+0.873\tan^{-1}\frac{W}{h}}\end{array}\right], \tag{12}$$

$$\frac{R_1}{Z_0} = 1.024\tanh\left(2.025\frac{W}{h}\right) \tanh\left[\begin{array}{l}\left(0.01584+0.0187\frac{h}{W}\right)\frac{S}{h}\\ +\left(0.1246+0.0394*\sinh\left(\frac{W}{h}\right)\right)\end{array}\right], \tag{13}$$

$$C_2 * \frac{25Z_0}{h} = \left[0.1776+0.05104\ln\left(\frac{W}{h}\right)\right]\frac{h}{S} + \left[0.574+0.3615\frac{h}{W}+1.156\ln\left(\frac{W}{h}\right)\right] \sec h\left(2.3345\frac{S}{h}\right), \tag{14}$$

$$L_2 * \frac{25}{hZ_0} = \left[0.00228+\frac{0.0873}{\cosh\left(\frac{W}{h}\right)+7.52\left(\frac{W}{h}\right)}\right] \sinh\left(2.3345\frac{S}{h}\right), \tag{15}$$

$$\frac{R_2}{Z_0}=\left[-1.78+0.749\frac{W}{h}\right]\frac{S}{h}$$
$$+\left[1.196-0.971\ln\left(\frac{W}{h}\right)\right]\sinh\left(2.3345\frac{S}{h}\right). \quad (16)$$

The equivalent circuit modeling procedure can be divided into two steps: produce S-parameter for the lack of coherence in the microstrip line and construct lumped circuit model which is independent of frequencies and describable using a set of equations based on physics of the structure. For the case in Fig. 4, the equivalent circuit satisfies a microstrip gap starting from a fraction until the gap approaches infinity.

Ground planes irregularity has very small effect on the coupled structure which can be ignored. The small microstrip rectangle in the middle of the ground plane works as the finite ground plane for the coupled microstrip lines of the patch.

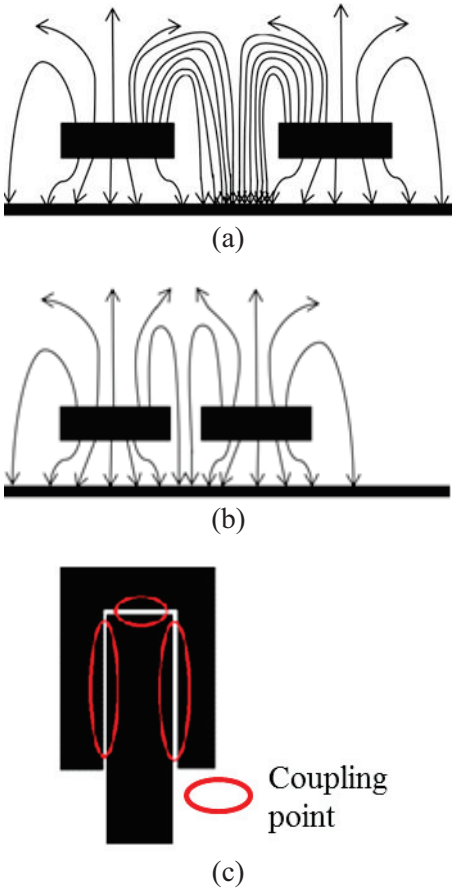

Fig. 3. (a) Coupled microstrip lines at a distance, (b) decreased gap between coupled lines, and (c) coupling points of the proposed antenna.

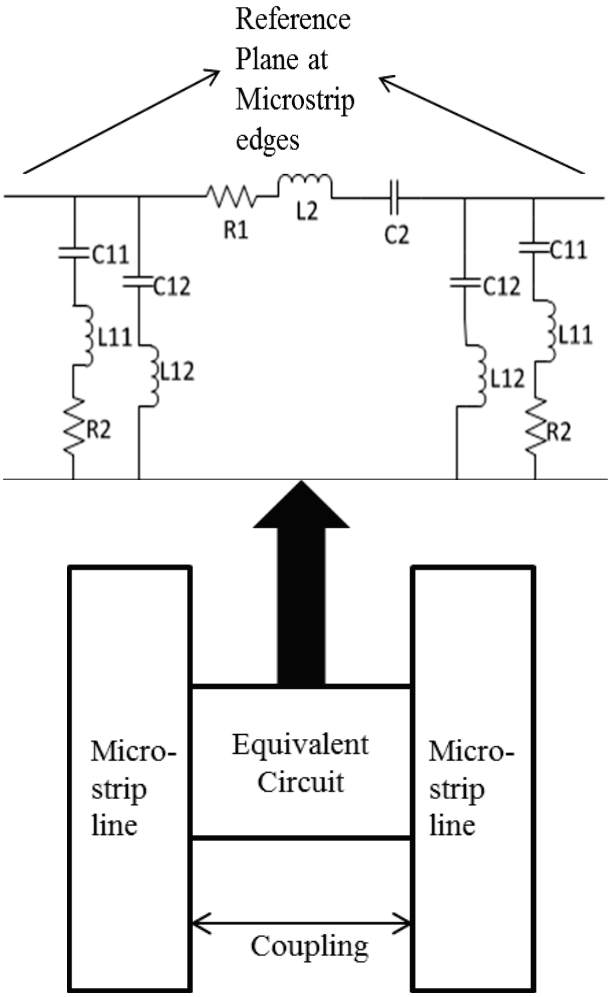

Fig. 4. Equivalent circuit of a microstrip coupled line gap.

The ground plane in Fig. 1 (b) has a circular slot in the middle which indicates the antenna can be classified as aperture type antenna. By Babbinet's principle, the complementary of that circular slot of the aperture type antenna radiation can be compared with the antenna radiation of a circular patch antenna. The principle is supported by the equations:

$$E_{\theta p}=H_{\theta c}, \quad (17)$$
$$E_{\varphi p}=H_{\varphi c}, \quad (18)$$
$$E_{\theta p}=-\frac{E_{\theta c}}{\eta_0^2}, \quad (19)$$
$$H_{\varphi p}=-\frac{E_{\varphi c}}{\eta_0^2}, \quad (20)$$

where, E_p=Electric field of circular patch, η_0=Intrinsic impedance of free space, E_c=Electric field of the complementary patch, H_p=Magnetic field of circular patch, and H_c=Magnetic field of complimentary patch. A microstrip rectangle is introduced in the middle of the circular slot in the ground plane.

Figure 5 shows the antenna along with its complementary structure:

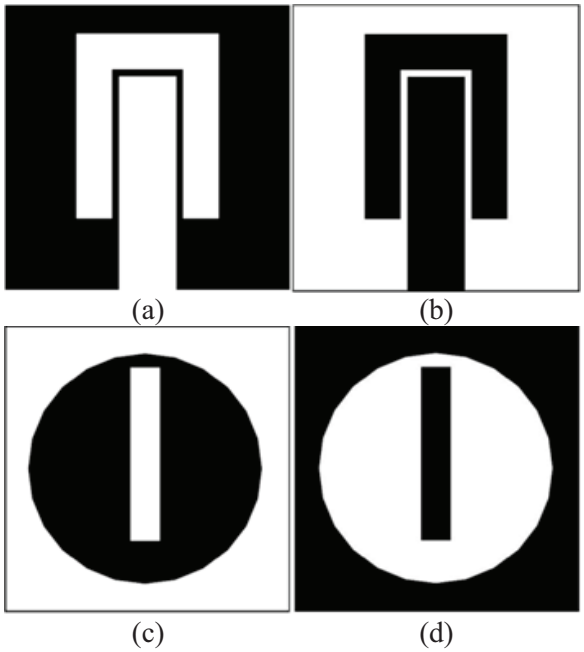

Fig. 5. (a) patch, (b) complementary of the patch, (c) ground plane, and (d) complementary of the ground plane.

The microstrip rectangle in the middle of the ground plane works as a finite ground for the coupled lines.

III. PARAMETRIC STUDIES

The antenna structure is simulated using a high and a low dielectric constant compared to FR4 substrate to investigate the behaviour of the planar structure for various existing substrate with same thickness, n=1.6 mm. Figure 6 shows the concluded study using different dielectric constant. Polyester with a dielectric constant, ε_{rp}=3.2 has a close relation (0.15 GHz first resonance frequency difference) with the S_{11} response of FR4 substrate. Moreover, Gallium Arsenide with a dielectric constant, ε_{rg}=12.9 shows a difference of 0.33 GHz with the primary resonance frequency of FR4. With high dielectric constant, the second resonance response of the antenna starts to degrade confirming that, FR4 is a valid choice for the proposed antenna design which is quite chip and available. Another widely used [21, 22] substrate from Rogers RO4350B with dielectric constant of 3.66 is compared in Fig. 5. The primary resonance response tends to shift 0.78 GHz towards frequency increment. From the discussions described, the observation is that the antenna design is more depended on the pattern of the microstrip lines over the substrate than the properties of substrate material itself.

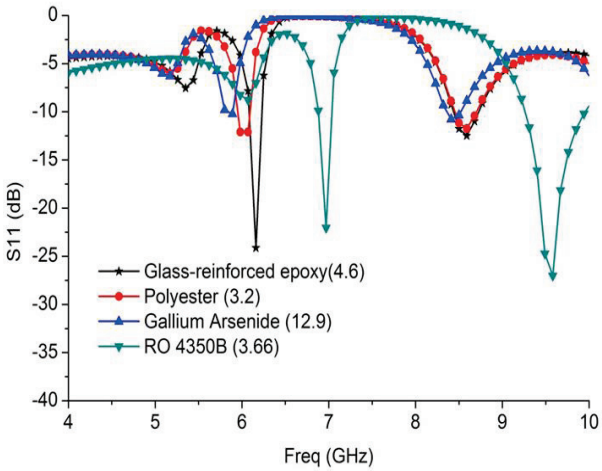

Fig. 6. S_{11} response with different dielectric constants.

Figure 7 shows a study of changing the radius 'R' of the circular slot at the ground plane. When R=6 mm the outer part of the circle already touches the microstrip rectangle situated in the middle and gives a lower frequency response at 4.51 GHz. The second resonance frequency however, fades away. R=7 mm follows the same resonance response as for R=6 mm. At R=9 mm, the first resonance shifts left but also loses its resonance behaviour which narrows at 5.89 GHz barely passing the first resonance. In the case of second resonance, the antenna shows 330 MHz bandwidth with a resonance at 8.05 GHz. The antenna resonance response shows a harmonic relation with the change of the circular slot radius which can be seen when R=10 mm. At R=10 mm, the first resonance shifts to 5.35 GHz with a -10 dB bandwidth of 120 MHz

with a second and a third resonance response at 7.96 GHz and 10 GHz.

Figure 8 shows the behaviour change with the change of length of microstrip rectangle in the middle of the ground plane. The copper line in the middle plays important role on controlling the first resonance of the antenna. The results show that if the length of 'j' is decreased, the first resonance is fully missed. Also, the placement of the microstrip rectangle is optimized manually.

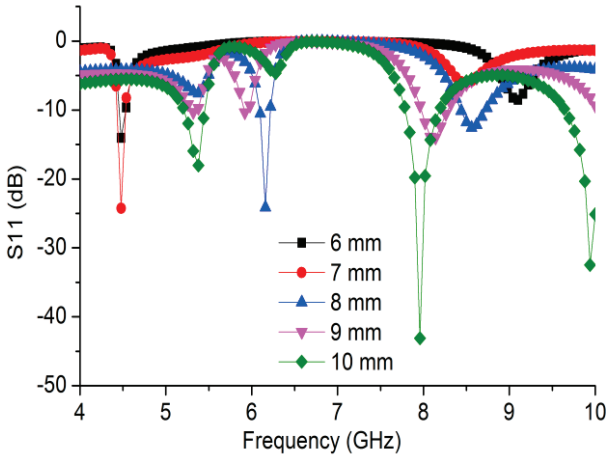

Fig. 7. Antenna resonance response with changed radius of circular slot.

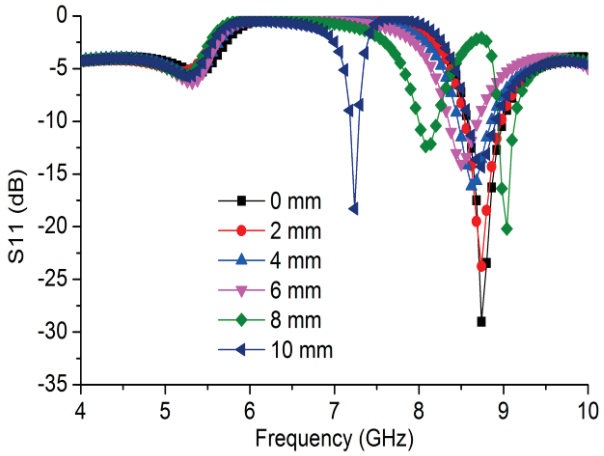

Fig. 8. Antenna resonance response with changed length of rectangle in the middle of the ground plane.

By changing the width 'k' of the microstrip rectangle in the middle of the ground plane, the behaviour change of resonance response found is shown in Fig. 9.

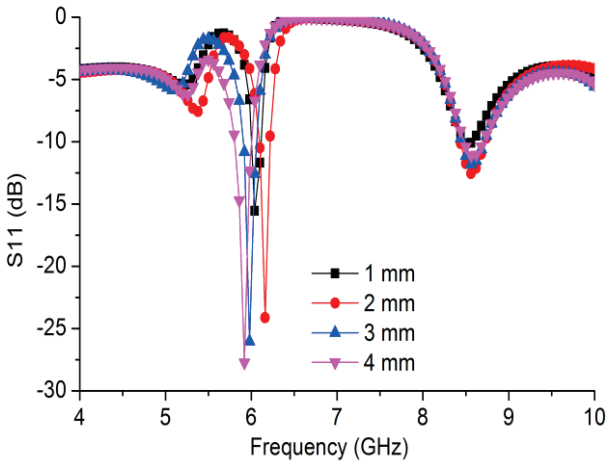

Fig. 9. Antenna resonance response with changed width of rectangle in the middle of the ground plane.

From the current distribution pattern, it can be seen that at the frequency 6.18 GHz, the current distribution over the strip line situated in the middle of the circular slot at the ground plane is high, as shown in Fig. 10, which also indicates a better result in that frequency. Minor perturbations can be seen at the patch of the antenna. By adjusting the length of the strip line in the ground plane, the resonance at 6.18 GHz can be tuned.

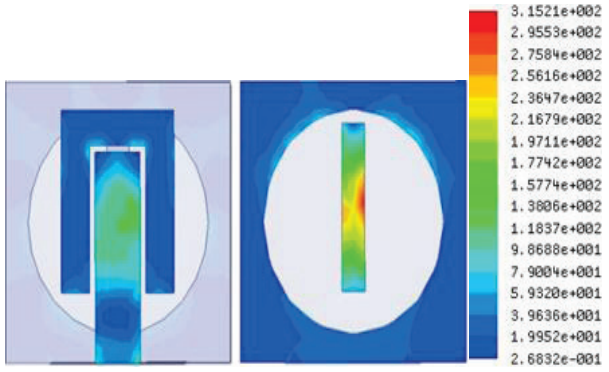

Fig. 10. Current distribution of the antenna at 6.18 GHz.

IV. OPTIMIZATION USING PSO ALGORITHM

PSO is a PSO based algorithm that is

specifically designed for antenna gain optimization. PSO can work with any finite number of variables given enough computation time [23]. Key problems with PSO are Curse of Dimensionality and Premature Convergence. The multi-start algorithm breaks the searching area into pieces of 2 and 3 dimensional spaces and edits it with a rapidly converging PSO. The multi-start technique removes the Premature Convergence issue completely. The k-dimensional breakdown approach improves the algorithm's performance highly dimensional problems. Until a predetermined termination criterion is met, the process is repeated up to a pre-determined number of iterations. PSO updates the particle position according to equations below:

$$v_{i+1} = wv_i + \varphi_1 r_1 (d_{localbest} - d_i) + \varphi_2 r_2 (d_{globalbest} - d_i), \quad (21)$$

$$d_{i+1} = d_i + v_{i+1}, \quad (22)$$

here, w=inertia coefficient, r_1, r_2=uniformly distributed random values between zero and one, v_i, d_i=velocity, dimensions of a particle at i^{th} iteration, φ_1, φ_2=cognitive and social coefficients.

The algorithm is modified for aperture type antenna design optimization. IE3D software is used to collaborate with the PSO algorithm executed in Matlab environment. A total number of 9 dimensions were optimized using this PSO algorithm.

The algorithm applied traditional PSO on 5 dimensions while holding the other dimensions constant. After 9 generations, the algorithm re-initialized the population and making two active dimensions inactive and replacing them two previously inactive dimensions. The swapping of active dimensions with inactive dimensions is done at random. After 246 generations, the optimized result is achieved. The pre-optimized and post-optimized dimensions are given in Table 1.

In this paper, the average gain and resonance over C-band and X-band was optimized; hence, it was the fitness function for this maximization problem. Figure 15 illustrates the improvement of the best fitness achieved during optimization. This validates the performance of the PSO.

Table 1: Design specification of the proposed antenna

Antenna Dimension	Before Optimization	After Optimization
Substrate	FR4	FR4
Relative permittivity of the substrate, (ε_r)	4.55	4.55
Thickness of the dielectric substrate, (n)	1.6 mm	1.6 mm
Ground plane (a × a)	20 mm × 20 mm	20 mm × 20 mm
Hands length of the coupling element, (b)	13.5 mm	16.2 mm
Hands length of the coupling element, (p)	13.5 mm	14.3 mm
Length of the primary patch, (c)	15 mm	16.9 mm
Distance from the boundary to coupling element, (d)	2 mm	0.15 mm
Gap between primary and coupling element, (e)	0.5 mm	0.61 mm
Distance from the boundary to the hand of the Coupling element, (f)	5 mm	6.2 mm
Width of the coupling element, (g)	2.5 mm	1.2 mm
Width of the coupling element, (q)	2.5 mm	1.23 mm
Width of the primary patch, (m)	4 mm	4 mm
Distance from the circular slot to the rectangle,(h)	1 mm	1 mm
Width of the rectangle, (k)	2 mm	2 mm
Length of the rectangle, (j)	12 mm	12 mm
Distance from the boundary to the rectangle, (i)	9 mm	9 mm
Radius of the circular slot, (R)	8 mm	8 mm

V. ANTENNA MEASUREMENT

The measurements of two antennae are done using Agilent PNA analyser with model no. E8358A. An anechoic chamber with length and width of 4.5 meter by 3.5 meter and a height of 4 meter is used to measure the polarization and gain of the antenna. A three antenna measurement technique is applied with a gap of 3 meter from each other. For the far field measurement, as the antenna is an electromagnetically short at 5.5 GHz, the minimum far field distance can be calculated as $d_f >> 2\lambda$. So, for this case, a 3 meter distance will serve the far field pattern quite nicely. Among three antennae two of the antennae are linearly polarized horn antennae with model no. SAS 571 and the other antenna is the AUT. At first the two antennae (horn antennae) with known gains are measured for the gain among each other and then the AUT is measured. The calculation based on Friis transmission equation demonstrates the calculation for the gain measurement shown in equation (13):

$$G_i dB + G_j dB = 20\log_{10}\left(\frac{4\pi R}{\lambda}\right) + 10\log_{10}\left(\frac{P_r}{P_t}\right)^k, \quad (23)$$

here, i=1, 2, 3, j=1, 2, 3, i≠j and k=1, 2, 3. R=distance between two antennae, P_t=transmitted power, P_r=received power, G=gain of the antenna.

VI. RESULTS OF THE DESIGNED ANTENNAE

Figure 11 shows the fabricated antennae using FR4 substrate with a thickness of 1.6 mm and a dielectric constant of 4.55. In Fig. 11 (a) shows the antenna fabricated before optimization and (b) shows the antenna after optimization.

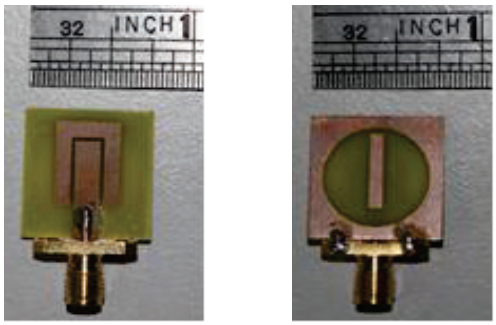

(a)

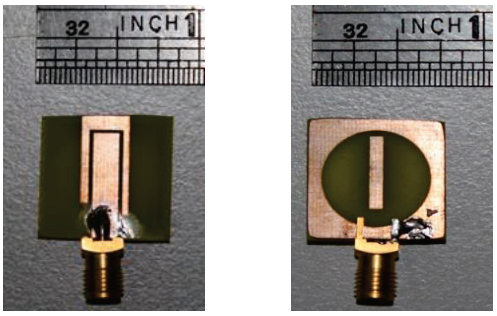

(b)

Fig. 11. (a) Antenna before optimization, and (b) antenna after optimization.

Clearly with naked eyes, it can be seen that there are changes in the pattern of the dimensions of the patch. The ground plane remains unchanged as no optimization algorithm was applied to the ground plane.

Figure 12 shows the resonance response of the antennae. The S_{11} response of the first antenna (before optimization) is less than -10 dB for the frequency starting from 5.89 GHz to 6.52 GHz with a notch at 6.25 GHz which degrades the total bandwidth performance of the antenna. Another resonance can be found starting at 8.71 GHz and ending at 8.77 GHz. The bandwidth at this resonance (X-band) is low. From the simulation results, it is clear that the second resonance is missed from the graph of the measured performance of the antenna before optimization.

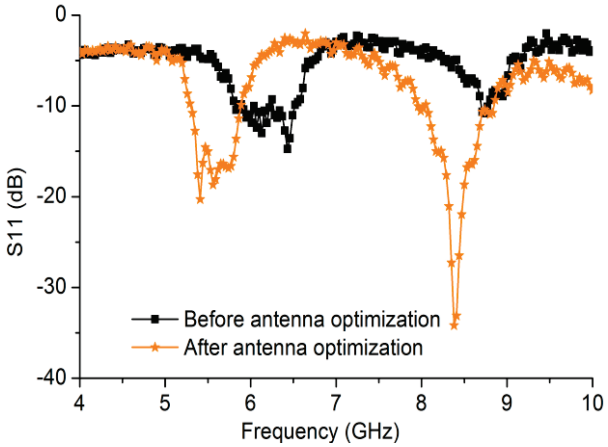

Fig. 12. Measured S_{11} response of the proposed multiband antenna.

After optimization, the resonance response of the optimized antenna can be found in Fig. 12. It is clear from the graph that the antenna is optimized to gain resonance frequency response at C-band and X-band with best bandwidth possible. A bandwidth of 0.6 GHz starting from 5.29 GHz to 5.89 GHz is achieved at the first resonance (C-band) [29], and a bandwidth of 0.93 GHz is achieved at the frequency starting from 7.93 GHz to 8.86 GHz (X-band). At C-band the lowest resonance response is less than -20 dB and at X-band the lowest resonance response is less than -34 dB. No notch is detected at the resonance frequency of the optimized antenna.

Figure 13 shows the measured gain of both the antennae. The gain of the antenna before optimization has an average gain of 2.7 dBi at the frequency starting at 6.05 GHz to 6.24 GHz with a peak gain of 4.07 dBi at 6.15 GHz. The range of frequency is quite low considering high gain at the resonance frequency. At the X-band, the gain is lower than 0 dBi for the first antenna.

For the optimized antenna, at C-band, the average gain starting from 5.29 GHz to 5.93 GHz is 3.2 dBi with a peak gain of 5.65 dBi at 5.84 GHz. At the X-band, with a high bandwidth a peak gain of 6.62 dBi is achieved at 8.16 GHz frequency. The average gain at X-band is 4.3 dBi starting from 7.93 GHz till 8.68 GHz.

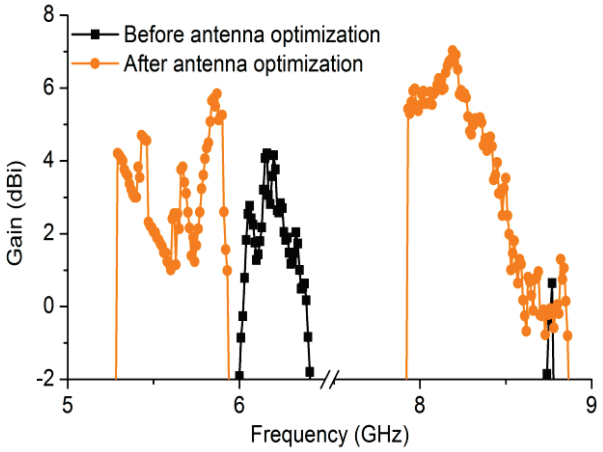

Fig. 13. Measured peak gain of the dual-band antenna.

Figure 14 shows the polarization of the optimized antenna at 5.5 GHz and 8.3 GHz. Observe that at 5.5 GHz in the E-plane, the antenna shows an omni-directional pattern at both co- and cross-pol. However, at 5.5 GHz, H-plane shows irregularity of co-polarization from 270° till 360°. Again for 8.3 GHz, the radiation pattern is somewhat omni-directional at the E-plane, whereas, at H-plane an irregularity can be seen at the co-pol which can be ignored due to the overall omni-directional performance.

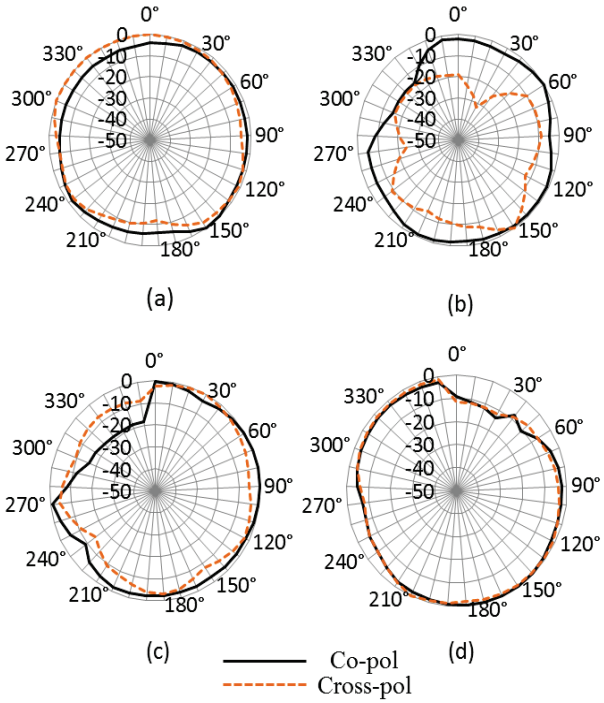

Fig. 14. Normalized radiation pattern of the antenna at: (a) 5.5 GHz (E-plane), (b) 8.3 GHz (E-plane), (c) 5.5 GHz (H-plane), and (d) 8.3 GHz (H-plane).

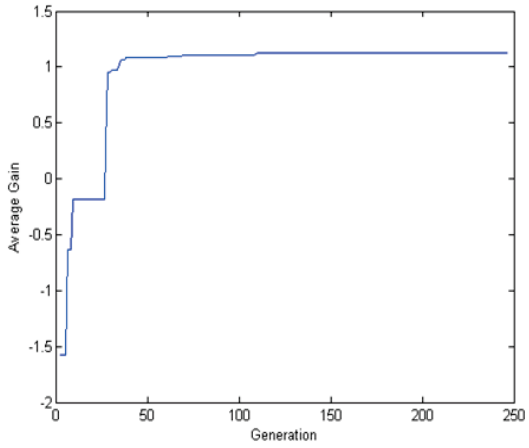

Fig. 15. Average gain increment after 246 generations (taken from Matlab).

VII. CONCLUSION

A new method for the design of microstrip patch antenna is described in this paper. A U-shaped parasitic element is introduced covering the active patch body of the antenna. The dimension of the patch and U-shaped element is optimized using modified PSO algorithm. Two antennae are fabricated to compare the result before and after the optimization were done. By changing the width of the U-shaped parasite, resonance frequency of the antenna can be changed. The antenna design is optimized for C-band and X-band frequency responses. After the optimization, the antenna at 5.84 GHz shows a maximum gain of 5.65 dBi and at 8.16 GHz the gain is 6.62 dBi. The resonance response of the antenna falls sharply at the desired frequencies of C-band and X-band. For future work, an array of this antenna can be proposed to have increased gain and more practical for the C-band and X-band applications.

REFERENCES

[1] M. Tzortzakakis and R. Langley, "Quad-band internal mobile phone antenna," *IEEE Trans. Antennas Propag*., vol. 55, no. 7, pp. 2097-2103, Jul. 2007.

[2] Y. Chi and K. Wong, "Compact multiband folded loop chip antenna for small-size mobile phone," *IEEE Trans. Antennas Propag*., vol. 56, no. 12, pp. 3797-3803, Dec. 2008.

[3] J. J. Tiang, M. T. Islam, N. Misran, et al., "Slot loaded circular microstrip antenna with meandered slits," *Journal of Electromagnetic Waves and Applications*, vol. 25, issue 13, pp. 1851-1862, 2011.

[4] K. Wong and C. Huang, "Printed loop antenna with a perpendicular feed for penta-band mobile phone application," *IEEE Trans. Antennas Propag*., vol. 56, no. 7, pp. 2138-2141, Jul. 2008.

[5] K-J. Kim, S-H. Lee, B-N. Kim, et al., "Small antenna with a coupling feed and parasitic elements for multiband mobile applications," *IEEE Antennas and Wirelesss Propagation Letters*, vol. 10, pp. 290-293, 2011.

[6] R. Azim, M. T. Islam, and N. Misran, "Printed planar antenna for wideband applications," *Journal of Infrared Millimeter and Terahertz Waves*, vol. 31, issue 8, pp. 969-978, 2011.

[7] X. Qu, Z. He, W. Shi, et al., "Multiband analysis of Sierpinski Gasket antenna with an iterative method," *Wireless Communications & Signal Processing, WCSP International Conference on*, pp. 1-4, Nov. 2009.

[8] J. Costantine, K. Y. Kabalan, A. El Hajj, et al., "New multi-band design for a microstrip patch antenna," *Antennas and Propagation, EuCAP, The Second European Conference on*, pp. 1-4, Nov. 2007.

[9] J. Costantine, C. G. Christodoulou, and S. E. Barbin, "A new reconfigurable multi band patch antenna," *Microwave and Optoelectronics Conference, IMOC, SBMO/IEEE MTT-S International*, pp. 75-78, Oct. 2007.

[10] L. Liu, S. Zhu, and R. Langley, "Dual-band triangular patch antenna with modified ground plane," *Electronics Letters*, vol. 43, issue 3, pp. 140-141, Feb. 2007.

[11] R. Azim, M. T. Islam, N. Misran, et al., "Planar UWB antenna with multi-slotted ground plane," *Microwave and Optical Technology Letters*, vol. 53, issue 5, pp. 966-968, 2011.

[12] B. Yildirim, "Multiband and compact WCDMA/WLAN antenna for mobile equipment," *IEEE Antennas and Wireless Prop. Letters*, vol. 10, pp. 14-16, 2011.

[13] K. Y. Lam, K-M. Luk, K. F. Lee, et al., "Small circularly polarized U-slot wideband patch antenna," *IEEE Antennas and Wireless Prop. Letters*, vol. 10, pp. 87-90, 2011.

[14] M. T. Islam, M. Moniruzzaman, N. Misran, et al., "Curve fitting based particle swarm optimization for UWB patch antenna," *Journal of Electromagnetic Waves and Applications*, vol. 23, issue 17-18, pp. 2421-2432, 2009.

[15] Y. Rahmat-Samii and N. Jin, "Particle swarm optimization (PSO) in engineering electromagnetics: a nature-inspired evolutionary algorithm," *ICEAA*, pp. 177-182, Sept. 2007.

[16] S. Singh, S. Tayal, and G. Sachdeva, "Evolutionary performance of BBO and PSO algorithms for Yagi-Uda antenna design optimization," *WICT 2012*, pp. 861-865, 2012.

[17] F. A. Ali and K. T. Selvan, "A study of PSO and its variants in respect of microstrip antenna feed point optimization," *Asia-Pacific Microwave Conf., 2009*, pp. 1817-1820, 2009.

[18] K. Y. Lam, K-M. Luk, K. F. Lee, et al., "Small circularly polarized U-slot wideband patch antenna," *IEEE Antennas and Wireless Prop. Letters*, vol. 10, pp. 87-90, 2011.

[19] M. N. O. Sadiku, *Boundary Conditions*, in Elements of Electromagnetics, 4th ed., New York, Oxford University Press, ch. 5, sec. 9, pp. 190, 2007.

[20] N. G. Alexopoulos and S. Wu, "Frequency-independent equivalent circuit model for microstrip open-end and gap discontinuities," *IEEE Transactions on Microwave Theory and Techniques*, vol. 42, no. 7, pp. 1268-1272, Jul. 1994.

[21] C-J. Hwang, L. B. Lok, I. G. Thayne, et al., "A wide bandpass filter with defected ground structure for wide out-of-band suppression," *Microwave Conference, Asia Pacific*, pp. 2018-2021, Dec. 2009.

[22] Y. M. Kempa, Z. E. Kazanivsky, H. H. Masyutin, et al., "Specific features of wide-band microwave filters constructive design," *Microwave & Telecommunication Technology*, pp. 481-483, Sept. 2007.

[23] M. Wu, "Improved intelligent optimization algorithm for the application of feedback design," *Journal of Convergence Information Technology*, vol. 6, no. 9, Sept. 2011.

[24] D. M. Pozar, *Microwave Engineering*, Edition 4, John Wiley & Sons, Inc., pp. 347.

[25] J. Zhang, X. Yang, J. Li, et al., "Triangular patch Yagi antenna with reconfigurable pattern characteristics," *Applied Computational Electromagnetics Society (ACES) Journal*, vol. 27, no. 11, pp. 918-924, Nov. 2012.

[26] Y. Li, W. Li, and W. Yu, "A multi-band/UWB MIMO/diversity antenna with an enhanced isolation using radial stub loaded resonator," *Applied Computational Electromagnetics Society (ACES) Journal*, vol. 28, no. 1, pp. 8-20, Jan. 2013.

[27] H. Oraizi and B. Rezaei, "Application of inductive loadings for the dual and broad banding of CPW-fed ring antennas," *Applied Computational Electromagnetics Society (ACES) Journal*, vol. 27, no. 7, pp. 587-595, Jul. 2012.

[28] P. Wang, G. Wen, and Y. Huang, "Compact CPW-fed planar monopole antenna with triple-band operation for WLAN/WiMAX applications," *Applied Computational Electromagnetics Society (ACES) Journal*, vol. 27, no. 8, pp. 691-696, Aug. 2012.

[29] *IEEE Standard Letter Designations for Radar-Frequency Bands*, IEEE Std. 521-2002 (Revision of IEEE Std. 521-1984), pp. 1-3, 2003.

[30] L. Liu, S. W. Cheung, et al., "A compact circular-ring antenna for utra-wideband applications," *Microwave and Optical Technology Letters*, vol. 53, issue 10, pp. 2283-2288, 2011.

[31] A. T. Mobashsher, M. T. Islam, et al., "Wideband compact antenna with partially radiating coplanar ground plane," *Applied Computational Electromagnetics Society (ACES) Journal*, vol. 26, no. 1, pp. 73-81, Jan. 2011.

[32] M. S. Alam, M. T. Islam, and N. Misran, "A novel compact split ring slotted electromagnetic bandgap structure for microstrip patch antenna performance enhancement," *Progress in Electromagnetic Research (PIER)*, vol. 130, pp. 389-409, 2012.

Md. Rokunuzzaman was born in Dhaka, Bangladesh in 1989. He was awarded his B.Eng. (Hons) Electronics majoring in Microwave and Communications from Multimedia University (MMU), Malaysia. Currently he is pursuing his M.Sc. degree in Universiti Kebangsaan Malaysia and worked as a Research Assistant at Centre for Space Science (ANGKASA) in a research project funded by Malaysian government. His research interest focuses on microstrip antenna design, MMICs, RFID passive tag antenna, microwave filter, microwave power divider, amplifier, telecommunication, wireless communication, etc.

Mohammad Tariqul Islam is a Professor in the Department of Electrical, Electronic and Systems Engineering of the Universiti Kebangsaan Malaysia (UKM). He is also the Group Leader of Radio Astronomy Informatics Group at UKM. Prior to joining UKM, he was a Lecturer in Multimedia University, Malaysia. He is a Senior Member of the IEEE, regular Member of Applied Computational Electromagnetic Society (ACES) and serving as the Editor-in-Chief of the International Journal of Electronics & Informatics (*IJEI*). Tariqul has been very promising as a Researcher, with the achievement of several International Gold Medal awards, a Best Invention in Telecommunication award and a Special Award from Vietnam for his research and innovation. Over the years, he has carried out research in the areas of communication antenna design, radio astronomy antennas, satellite antennas, and electromagnetic radiation analysis. His publications include over 160 research journal papers, nearly 150 conference papers, and few book chapters on various topics related to antennas, microwaves and electromagnetic radiation analysis with 8 inventory patents filed. Thus far, his publications have been cited 1578 times, and the H-index is 24 (Source: Scopus). For his contributions, he has been awarded "Best Researcher Award" in 2010 and 2011 at UKM. He is now managing many research projects from the Ministry of Science, Technology and Innovation (MOSTI), Ministry of Higher Education Malaysia (MOHE) and some

International research grants from Japan.

Salehin Kibria was born in Dhaka, Bangladesh in 1988. He was awarded his B.Eng. (Hons) Electronics majoring in Telecommunications from Multimedia University (MMU), Malaysia. He was awarded his M.Sc. degree in Universiti Kebangsaan Malaysia and employed as a Research Assistant at Centre for Space Science (ANGKASA) in a research project funded by Malaysian government. His research interest focuses on RFID Reader Antenna designs, telecommunication, Particle Swarm Optimization, etc.